Applied Energy 376 (2024) 124167

Contents lists available at ScienceDirect

Applied Energy

journal homepage: www.elsevier.com/locate/apenergy

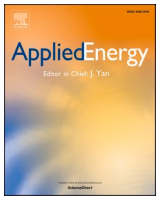

Techno-economic assessment for the practicability of on-board CO_2 capture in ICE vehicles

Alexander García-Mariaca [a,*], Eva Llera-Sastresa [b]

[a] Energy and CO_2 Group, Department of Mechanical Engineering, Aragon Institute of Engineering Research (I3A), University of Zaragoza, Zaragoza 50018, Spain
[b] Department of Mechanical Engineering and CIRCE Research Institute, University of Zaragoza, María de Luna s/n, Zaragoza 50018, Spain

HIGHLIGHTS

- Thermal study for dimensioning the CCS-ORC system operating in HD-ICEV.
- Techno-economic assessment of a novel CCS-ORC system for operation in HD-ICEV.
- CAC less than 35 €/tCO_2 for a carbon capture rate of 100 %.
- CCS-ORC system would be profitable with a CO_2 tax above of 80 €/tCO_2.

ARTICLE INFO

Keywords:
Carbon capture and storage
Temperature swing adsorption
Organic Rankine Cycle
Decarbonisation
Transport sector

ABSTRACT

The transport sector is a major energy-intensive and significant contributor to CO_2 emissions. With heavy-duty internal combustion engine vehicles (HD-ICEVs) set to remain a primary mode of transport for goods and passengers, the European Union plans to implement CO_2 emission rights starting in 2027 to address this issue. To mitigate CO_2 emissions, on-board carbon capture technologies can be an innovative solution, but a comprehensive analysis from several perspectives must be carried out. To tackle the existing knowledge gap on this subject, this paper presents the techno-economic assessment of a CO_2 capture and storage system hybridised with an organic Rankine cycle (CCS-ORC) integrated into an HD-ICEV whose technical ability has been previously demonstrated. In this paper, the capture installation based on temperature swing adsorption is designed for two engines with different displacement volumes, at varying carbon capture rates (CCR), and using three different sorbents. The size of the thermal devices is estimated as the determinant factor for the required space and the installation costs. The results show that the heat exchangers can achieve a minimum area density of 100 m^2/m^3, while the most significant temperature swing adsorption device obtained is scarcely 0.26 m^3. The carbon abatement cost (CAC) obtained for the CCS-ORC system is less than 35 €/tCO_2 at 100 % of CCR, and with an engine size greater than 18 and 21 L, the CAC of the CCS-ORC system is zero at 100 and 70 % of CCR, respectively. Furthermore, with a CO_2 emissions right price above 71 €/tCO_2, the projected payback of the initial investment of the CCS-ORC system is achieved in the lifespan of the HD-ICEV for all sorbents evaluated at 100 % of CCR.

1. Introduction

As the world addresses the pressing challenge of climate change, finding innovative solutions to reduce carbon emissions has become forefront. For this reason, in recent years, much research has been conducted to tackle this problem in several intensive energy sectors [1]. One of the sectors where great interest has been aroused in the development of carbon capture and storage (CCS) systems is the transport sector, notably in ships and heavy-duty road vehicles. This heightened interest is primarily driven by the fact that this sector alone is accountable for generating 7.98 Gt of CO_2 in 2022. constituting 23 % of the global CO_2 emissions for this year [2].

Nonetheless, developing an on-board CCS system for vehicles in road freight transport propelled by internal combustion engines (ICE) confronts numerous challenges. These include the necessity for adaptability to diverse engine operations, encompassing variations in engine load (EL) and rpm. Moreover, such a system must meet stringent criteria; it

* Corresponding author.
E-mail address: alexander.garcia@unizar.es (A. García-Mariaca).

https://doi.org/10.1016/j.apenergy.2024.124167
Received 16 April 2024; Received in revised form 24 July 2024; Accepted 6 August 2024
Available online 27 August 2024

Abbreviations

β	Area density
B	Baffles
CAPEX	Capital expenditure
CAC	Carbon abatement cost
CCS	Carbon Capture and Storage
CCR	Carbon Capture rate
C′	Clearance between tubes
η_{com}	Combustion efficiency
CNG	Compressed natural gas
h	Convection heat transfer coefficient
HE-CO_2-C	CO_2 cooling heat exchanger
CO_2-con	CO_2 condenser
CO_2-com	CO_2 compressor
C_5H_{10}	Cyclopentane
f	Darcy friction factor
ρ	Density
S_D	Diagonal pitch
D	Diameter
V_d	Displacement volume
μ	Dynamic viscosity
EB	Electric batteries
η_{eng}	Engine efficiency
EL	Engine load
D_e	Equivalent diameter
EG	Exhaust gases
HE-EG1	Exhaust gas cooling heat exchanger 1
HE-EG2	Exhaust gas cooling heat exchanger 2
Fr	Froude number
HD-ICEV	Heavy-duty internal combustion engine vehicles
HFCB	Hydrogen fuel cell batteries
ICE	Internal Combustion Engine
Ja	Jacob number
h_{fg}	Latent heat of vaporization
S_L	Longitudinal pitch
LHV	Lower Heating Value
$\dot{m}$	Mass flow
NPV	Net present value
q_s	Nucleate boiling heat
Nu	Nusselt number
ORC-C	ORC condenser
ORC-E	ORC evaporator
ORC-H	ORC heater
ORC-P	ORC pump
ORC-X	ORC expander
ORC	Organic Rankine Cycle
U	Overall heat coefficient
PP	Power penalty
Pr	Prandtl number
R	Radius
Re	Reynolds number
T_{sat}	Saturation temperature
Sc	Schmidt number
c_p	Specific heat
$G_{s,f}$	Surface-fluid combination
Σ	Liquid surface tension
TSA	Temperature Swing Adsorption
K	Thermal conductivity
T	Time
S_T	Transverse pitch
P_t	Tube pitch
$\overline{X}$	Vapour mass fraction
WHTC	World Harmonized Transient Cycle

Subscripts

i	Inner or inlet
l	Liquid
o	Outlet
s	Property evaluated at surface temperature
v	Vapour

should be practical, efficient, and reliable, and it must be seamlessly integrated into existing vehicles with minimal impact on their usable volume. Above all, the effects of its operation on the engine's performance should be as minimal as possible. Furthermore, any investment in a CCS system must demonstrate economic viability for vehicle owners, i.e., the additional investment incurred through system installation should have a payback at least over the vehicle's lifespan.

In this regard, numerous researchers have been developing innovative research works on this topic. Consequently, significant progress is being made in the concept design of CCS systems operating in heavy-duty internal combustion engine vehicles (HD-ICEV). These initial approaches have introduced well-established technologies, such as amine scrubbing [3,4], temperature, pressure, or vacuum swing adsorption (TSA, PSA, and VSA), for on-board CO_2 capture [5]. Moreover, specific research endeavours have implanted auxiliary systems primarily to offset the power demand in CO_2 compression, such as organic Rankine cycles (ORC) that take advantage of the waste heat in the exhaust gases [6,7]. From these research works, different configurations of the CCS system have been obtained [5,8], the performance of the CCS system operating with various sorbents has been evaluated. It has been determined that the operation of the CCS system at a carbon capture rate (CCR) of 100 % requires an average less than 10 % of the power produced by the engine [9]. However, in the literature, no study has performed an in-depth techno-economic analysis of a CCS system operating in an HD-ICEV.

In this sense and in pursuit of advancing the continuous development of this technology, this research carries out the first techno-economic assessment of a CCS system operating in an HD-ICEV. The techno-economic evaluation is based on the energy assessment results from a previous investigation of a CCS system with an integrated ORC (CCS-ORC system onwards) capable of operating under different load and rpm conditions of heavy-duty engines [9]. The conceptual design is mainly based on knowing in detail the configuration of the heat exchangers (number of tubes and lengths and arrangement). Subsequently, the compaction of these exchangers is calculated, which must satisfy the heat transfer parameters found in the simulations done in the previous study.

The initial variable calculated in the techno-economic assessment of the CCS-ORC system is the capital expenditure (CAPEX), which is then compared with other zero-emission technologies available in heavy-duty vehicles, such as hydrogen fuel cell batteries (HFCB) and electric batteries (EB). Subsequently, the operational expenditures (OPEX), the income obtained by avoiding paying the CO_2 emission tax, the profits and the carbon abatement cost (CAC) by introducing a CCS-ORC in an HD-ICEV system are obtained. Finally, with these results, a sensitivity analysis is carried out to determine the suitable value of the CO_2 emissions rights and the engine size so that the CCS system investment recovers as soon as possible. The key indicators for this study are the CCR (100 and 70 %), the kind of sorbent (PPN-6-CH_2-DETA, MOF-74-Mg and activated carbon) and the engine size (engine volume displacement). The outcomes of this research endeavour are vital to continue closing the knowledge gap about CCS systems operating in HD-ICEV, thereby

advancing technologies conducive to achieving complete decarbonization of the transport sector in the medium term.

2. Methodology

The procedures described in this section show the steps for obtaining the conceptual design and economic assessment of an innovative CCS-ORC system designed to operate on-board a natural gas-fuelled HD-ICEV. The methodology begins with selecting the vehicles, followed by a comprehensive description of the CCS-ORC system, heat exchanger sizing, and design of the TSA device and concludes with economic considerations.

2.1. Vehicle selection

The vehicles selected for the present research are the Citaro bus and the IVECO Daily VAN, whose engines are the M936G and the F1C, respectively. Both engines are turbocharged natural gas internal combustion engines. The simulation of engine performance and emissions parameters was conducted using the AVL software. The outcomes of these simulations, along with the technical specifications of the engines, are presented herein [8].

2.2. Description of CCS-ORC system and assessment conditions

Fig. 1 depicts the schematic representation of the CCS-ORC system proposed. The system comprises four distinct zones. The first one is dedicated to the processes of adsorption and desorption of CO_2 through a temperature swing of the sorbent (TSA). In this zone, the exhaust gases' waste heat is harnessed to heat the sorbent and desorb CO_2. The second zone encompasses the ORC, which takes the remaining waste heat from the exhaust gases to generate power. This power is then utilized to meet the energy demands of the CO_2 compression. The ORC comprises three heat exchangers (condenser, heater and evaporator), a pump, an expander, and a tank. The working fluid in the ORC is cyclopentane (C_5H_{10}), which was chosen due to its outstanding performance in prior research on ORC in ICE [10,11]. The third zone involves conditioning exhaust gases by cooling them until dry, consisting of two heat exchangers and a cyclone. The final section is focused on CO_2 storage and encompasses two heat exchangers, a CO_2 compressor and a CO_2 tank for its storage. All zones are cooling with air that is supplied by a fan.

The energy analysis of the proposed CCS-ORC system was carried out with three different sorbents: PPN-6-CH_2-DETA (PPN onward), MOF-74-Mg (MOF onwards), activated carbon (AC onward), and two CCR 70 and 100 %. The results of the energy analysis are available in a prior study [9], which serves as the foundation for the techno-economic assessment presented in this paper. On that basis, the CCRs are kept, as well as the sorbents, which have a low adsorption heat is low [12], that is imperative for this application. Additionally, PPN and MOF exhibit high CO_2 loadings and CO_2/N_2 selectivity compared to AC, which has lower CO_2/N_2 selectivity and CO_2 loadings [13]. This allows for a comprehensive mapping of the evaluated variables and enables the extrapolation of results to other sorbents whose range of selectivity and CO_2 loadings are in the range of the evaluated sorbents.

2.3. Heat exchanger sizing

As shown in Fig. 1. the CCS-ORC system features seven heat exchangers, the areas of which were determined through energy modelling conducted in ASPEN+ [9]. However, a detailed design process is imperative to validate the results obtained in ASPEN+ and, in this way, ascertain the heat exchangers' cost. The assumptions for the calculations include: i) heat exchangers operating in cross-flow, ii) consideration of fully developed fluids, iii) the heat exchangers operating in steady-state conditions, iv) The fluids' inlet and outlet temperatures and mass flows of each fluid in the heat exchanger are taken at maximum power and engine load (see values for each heat exchanger, sorbent and engine in Appendixes A, B and C) and v) states' properties are calculated with the pressure and temperature averages at the inlet and outlet of each heat exchanger.

First, the Reynolds number for each fluid is obtained using Eq. 1. Once the flow regime for each fluid is determined, appropriate correlations are chosen to calculate the Nusselt number. Zukauskas' correlations for external convection in a flow cross-tube bank heat exchanger with staggered tube arrangement are employed for the shell side. The disposition of pipes is illustrated in Fig. 2. Table 1 outlines the correlations for each heat exchanger and the corresponding operating fluid (Eqs. 2 and 3).

$$Re = \frac{\rho V D}{\mu} \tag{1}$$

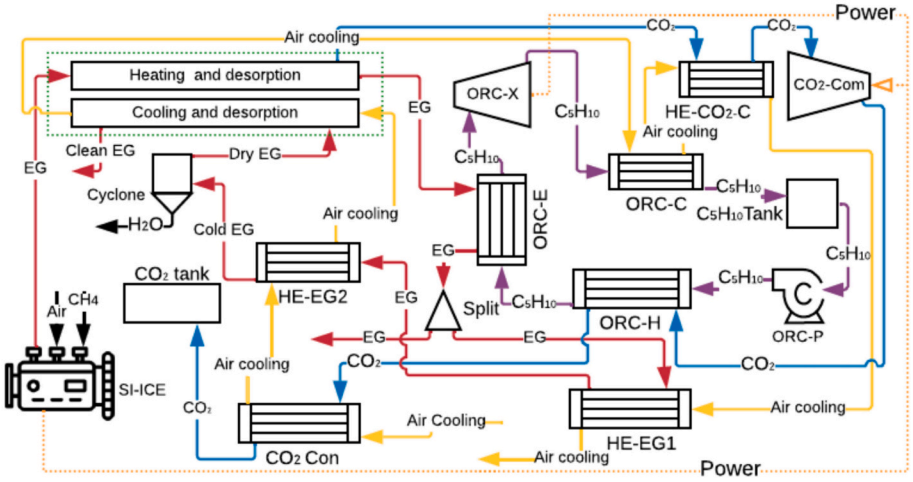

Fig. 1. CCS-ORC system schematic layout.

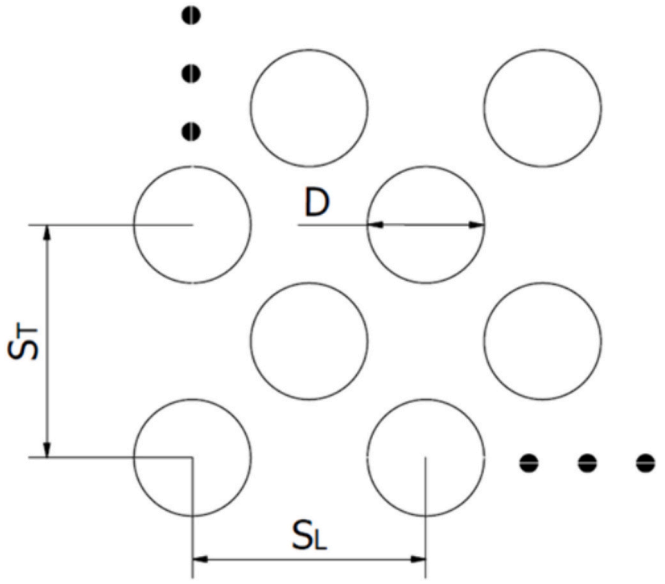

Fig. 2. Staggered disposal tube in the heat exchangers.

Within the annular section, the choice of correlation for Nusselt number computation is contingent upon the nature of the fluid process (heating, cooling, or condensing) and the fluid regime, which, in all instances, is turbulent. Table 2 delineates the selected correlation for each heat exchanger calculation (Eqs. 4 and 5). In each instance, a verification process was conducted to ensure that the constraints associated with each correlation were satisfied. Finally, for all cases enumerated in Table 2. the convection heat transfer coefficient (h) is obtained utilizing Eq. 6.

$$h = \frac{Nuk}{D} \tag{6}$$

The evaporative process of C_5H_{10} conducted within the ORC evaporator (ORE-E) exhibits a significantly elevated Reynolds number. The correlation identified in the literature to fit this condition is presented in Eq. 7 [17]. As delineated in the said equation, h is contingent upon the stratification parameter, $f(Fr)$, whose value is the unity for vertical tubes and horizontal tubes with Fr $\geq$ 0.04 [18], as is applicable in the present case. The surface-fluid combination ($G_{s,f}$) also influences h; the value of this latter oscillates between 1 and 2 for copper pipes and various refrigerants [17]. Consequently, a value of 1.5 for the current procedure is taken. Also, h is contingent upon the mean vapour mass fraction ($\overline{X}$), computed using Eq. 8. The value of x taken is half the length of a pipe in the heat exchanger. The nucleate boiling heat (q_s) also affects the behaviour of h, which is determined through the correlation established by Rohsenow (Eq. 9) [19]. In this equation, the coefficients C_{sf} and the exponent n rely upon the surface and fluid combination, with assigned values of 0.0154 and 1.7, respectively, corresponding to the n-pentane-copper polished configuration [20]. Finally, the h_{sp} is calculated with Eq. 4 with the fluid properties evaluated with the C_5H_{10} saturation temperature.

$$h_{eva} = \left[0.6683\left(\frac{\rho_{C_5H_{10},l}}{\rho_{C_5H_{10},v}}\right)^{0.1}\overline{X}^{0.16}(1-\overline{X})^{0.64}f(Fr) + 1058\left(\frac{A_c q_s}{\dot{m}_{C_5C_{10}}h_{fg}}\right)^{0.7}(1-\overline{X})^{0.8}G_{s,f}\right]h_{sp} \tag{7}$$

$$\overline{X} = \frac{q_s \pi D x}{\dot{m}_{C_5H_{10}}h_{fg}} \tag{8}$$

$$q_s = \mu_{C_5H_{10},l}h_{fg}\left[\frac{g\left(\rho_{C_5H_{10},l}-\rho_{C_5H_{10},v}\right)}{\sigma}\right]^{0.5}\left(\frac{c_{p,l}\Delta T_e}{C_{sf}Pr_l^n}\right)^3 \tag{9}$$

In contrast, the CO_2 liquefaction process in the CO_2 condenser (CO_2-Con) exhibits a low Reynolds number. In response to this, a correlation found in the literature allows calculation h directly (Eq. 10) [21], where the latent heat of vaporization (h_{fg}) is modified as is shown in Eq. 11.

$$h_{c,CO_2} = 0.555\left[\frac{g\rho_{CO_2,l}\left(\rho_{CO_2,l}-\rho_{CO_2,v}\right)k_{CO_2,l}{}^3h'_{fg}}{\mu_{CO_2,l}\left(T_{CO_2,out}-T_s\right)D}\right]^{1/4} \quad Re < 35000 \tag{10}$$

$$h'_{fg} = h_{fg} + \frac{3c_{p,l}(T_{sat}-T_s)}{8} \tag{11}$$

The determination of the overall heat transfer coefficient (U) is achieved through the application of Eq. 12; for this, it is used a fouling

Table 1
Correlation to obtain the Nusselt number in the shell side.

Heat exchanger	Fluid	Nusselt Correlation	Restriction	source
ORC-H ORC-E ORC-C HE-CO_2-C HE-EG1 HE-EG2	CO_2 EG Air Air Air Air	$Nu = 0.35\left(\frac{S_T}{S_L}\right)^{0.2}Re^{0.6}Pr^{0.36}\left(\frac{Pr}{Pr_s}\right)^{0.25}$ (2)	$0.7 < Pr < 500$ $1000 < Re < 2x10^5$	[14]
CO_2-Con	Air	$Nu = 0.031\left(\frac{S_T}{S_L}\right)^{0.2}Re^{0.8}Pr^{0.36}\left(\frac{Pr}{Pr_s}\right)^{0.25}$ (3)	$0.7 < Pr < 500$ $2x10^5 < Re < 2x10^6$	

Table 2
Correlation to obtain the Nusselt number in the annular section.

Heat exchanger	Process	Fluid	Nusselt Correlation	Constraints	Source
ORC-H HE-CO_2-C HE-EG1 HE-EG2	Heating Cooling 	C_5H_{10} CO_2 FG FG	$Nu = \frac{f/8(Re-1000)Pr}{(1+12.7(f/8^{0.5}(Pr^{2/3}-1))}$ (4)	$0.5 \leq Pr \leq 2000$ $3000 < Re \leq 5\ X\ 10^6$	[15]
ORC-C	Condensing	C_5H_{10}	$Nu = 0.85Re_v^{0.11}Re_l^{0.45}Ja^{-0.12}Sc^{-0.45}$ (5)	$0.07 \leq Ja \leq 0.34$ $0.7 \leq Sc \leq 2.2$ $Re > 35000$	[16]

factor is outside and inside in the heat exchanger of 4×10^{-4} and 2×10^{-4} m^2K/W, corresponding to air and working fluid values [22], respectively. The heat of each heat exchanger is calculated using Eq. 13 where the ΔT_{ln} is the mean temperature logarithm.

$$U = \frac{1}{\frac{1}{h_i} + 2\pi r_i L R_i + \frac{r_i}{k} ln\left(\frac{r_o}{r_i}\right) + 2\pi r_i L R_o + \frac{r_i}{r_o h_o}} \tag{12}$$

$$\dot{Q} = UA\Delta T_{ln} \tag{13}$$

Finally, the area density (β) is determined. This variable represents the relation between the required area and volume of the heat exchanger to contain the tube arrangement. The determination of heat exchanger size encompasses design variables such as the number, diameter, and length of tubes for each heat exchanger and sorbent operating in the CCS-ORC system. Additionally, the calculation includes a restriction in the tube length; this must not exceed 0.6 and 0.5 m for the heat exchangers of the CCS-ORC system that will be integrated into vehicles equipped with M936G and F1C engines, respectively. All these calculations are conducted in EES software, in which the U values for each heat exchanger must be a maximum variation of ±2 % with the results obtained in [9].

2.4. Design of the TSA device

Due to the lack of information about the cost of devices that carry out the TSA process in CO_2 capture, the design procedure of a TSA device is presented in this research, thereby facilitating the estimation of its manufacturing cost. The TSA device adopts a configuration reminiscent of a shell-and-tube heat exchanger. The bed sorbent is situated within the tubes, and the hot exhaust gases or the air-cooling flow in the shell (depending on the process developed). Fig. 3 shows a cross-sectional representation of the TSA device.

The sizing of the device begins with determining the maximum radius of the sorbent bed, whose geometry is cylindrical. A transient state heat transfer mathematical model is employed to achieve this. The model is made in the radial direction to simplify it (Eq. 14) and situated at the outlet of the bed sorbent due to it knowing the exhaust gases temperature at this point, which is the lowest temperature achieved in the desorption process (Table 3), so if the centre of the sorbent is obtained the desorption temperature required (150 °C [12]) it is guaranteed that of sorbent bet have this or even exceeded the desired temperature within a specified timeframe.

The boundary conditions governing the resolution of this equation involve a specular image at the centre (Eq. 15) and a convection boundary condition at the surface (Eq. 16). Finally, the initial condition stipulated is a sorbent temperature of 25 °C. The discretization of these equations is explained in Appendix D.

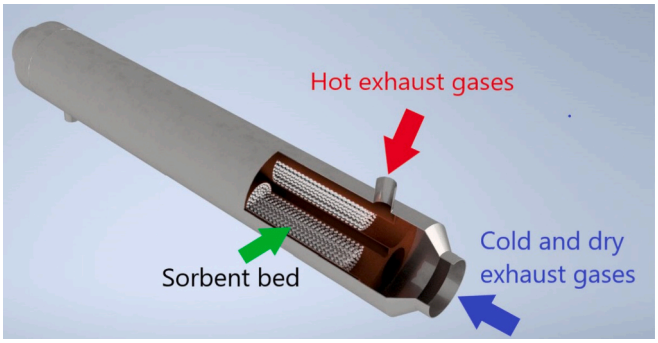

Fig. 3. Cross-sectional view of TSA device.

Table 3
Sorbent properties and temperature conditions used in the heat transfer mathematical model.

Engine	F1C	M936G	F1C	M936G	F1C	M936G
Sorbents	AC		MOF		PPN	
T_i at 25 % EL [°C]	428.55	481.25	428.55	481.25	428.55	481.25
T_o at 25 % EL and 100 CCR [°C]	221.85	275.53	260.33	313.85	222.02	275.70
T_o at 25 % EL and 70 CCR [°C]	285.01	338.42	311.57	364.85	285.13	338.53
c_p [J/kgK] [12]	1062		985		896	
k [W/mK]	0.36 [23]		0.52 [24]		0.3 [25]	
CO_2 loading [kg_{CO2}/kg_{sor}] [12]	0.132		0.278		0.235	
ρ [kg/m^3] [12]	1140		812.88		805	

$$\frac{k}{r}\left(\frac{\partial}{\partial r} r \frac{\partial T}{\partial r}\right) = \rho C_p \frac{\partial T}{\partial t} \tag{14}$$

$$2k\frac{\partial^2 T}{\partial r^2} = \rho C_p \frac{\partial T}{\partial t} \tag{15}$$

$$-k\frac{\partial T(r,t)}{\partial t} = h(Tinf - T(r,t)) \tag{16}$$

The heat transfer model assumes constant thermal conductivity and specific heat for the sorbent. Moreover, the density employed is half of each sorbent's crystallographic density. The Nusselt number is computed by following the procedure outlined in section 2.3 but utilizing Eqs. 17, 18, 19 and 20, which are used for a shell-tube heat exchanger on the shell side [26]. Ultimately, the h value is determined using Eq. 6.

$$A = \frac{D_{shell} C' B}{P_t} \tag{17}$$

$$D_e = \frac{4\left(P_t{}^2 - 0.25\pi d_o{}^2\right)}{\pi d_o} \tag{18}$$

$$Re = \frac{D_e \dot{m}_{EG}}{A\mu} \tag{19}$$

$$Nu = 0.027 Re^{0.8} Pr^{\frac{1}{3}} (\mu/\mu_w)^{0.14} \tag{20}$$

As delineated in these equations, the 'h' coefficient is contingent upon several parameters, including the distance between baffles in the shell (B), the clearance between tubes (C'), the tube pitch (P_t), the equivalent diameter (D_e), and the mass flow rate of exhaust gases. To facilitate these computations and determine the viscosities and Prandtl numbers, the values of mass flow and temperature are selected at the critical operational condition of the engine, specifically at the lowest rpm and engine load. The exhaust gas mass flow at those points is 66.9 kg/h for the F1C engine and 208.4 kg/h for the M936G engine, while the corresponding temperature values are detailed in Table 3.

The sorbent mass is calculated based on the CO_2 mass flow at the average operational points of the engines within the World Harmonized Transient Cycle (WHTC) [27]. Precisely, these points correspond to 1300 rpm for the M936G engine and 2000 rpm for the F1C engine, both at 25 % of the engine load. The corresponding CO_2 mass flow values are 44.96 kg/h for the M936G engine and 22.29 kg/h for the F1C engine. Fig. 4 illustrates the step-by-step calculation process. Based on the acquired results, the TSA device's geometry is obtained, and its surface area is taken for the TSA device's cost as if it were a heat exchanger. This process is conducted for each condition of the CCR and sorbent.

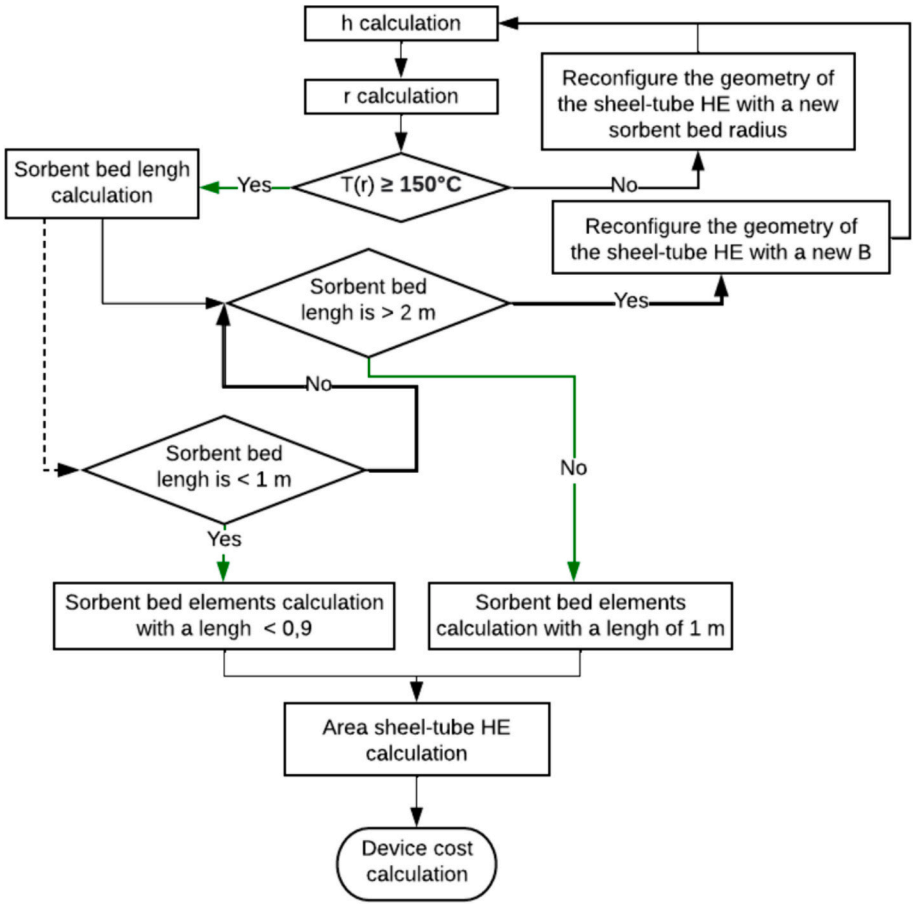

Fig. 4. Flowchart for calculation of the TSA device cost

2.5. Economical assessment

The economic analysis aims to determine the capital expenditure (CAPEX) of the CCS-ORC system. In this sense, the CAPEX is the sum of the costs of all components of the CCS-ORC system and the sum of direct and indirect costs (Eq. 21). The direct cost is associated with the installation, instrumentation, piping, and electric installation, and their value is a percentage of the sum of all equipment [28]. Subsequently, the indirect costs, which encompass engineering and contingency costs, are also computed as a percentage of the cumulative expenses incurred by all devices and direct costs [29].

$$CAPEX = \sum Cost_{Equipment} + \sum Cost_{direct} + \sum Cost_{indirect} \quad (21)$$

Device costs are obtained through correlations, depending on key variables governing their operation or geometric parameters. In the case of the compressor, expander, pump and fan, the primary variable is the power consumed or produced. In the case of heat exchangers, the heat exchanger area is the primary variable, and in the case of tanks, the function is the tank volume. The correlations utilized to ascertain the CAPEX of the CCS-ORC system are delineated in Table 4, and each

Table 4
CAPEX cost correlations and parameters.

Process	Equipment	Cost correlation	Parameter (A)	Ref.
TSA	TSA-Device	$3397A^{0.86}$	Area (m^2)	[30–32]
Waste heat recovery (ORC)	ORC-expander	$10^{\{2.2476+1.4965log_{10}(A)+0.1618[log_{10}(A)]^2\}}$	Volume (m^3)	[33]
	ORC-pump	$900(A/300)^{0.25}$	Power (kW)	
	ORC-C_5H_{10} tank	31.5 + 16A	Volume (L)	
	ORC-Evaporator	190 + 310A	Area (m^2)	
	ORC-heater	190 + 310A	Area (m^2)	[34]
	ORC-condenser	190 + 310A	Area (m^2)	
Exhaust gases condition (EGC)	HE-EG1	190 + 310A	Area (m^2)	
	HE-EG2	190 + 310A	Area (m^2)	
	Cyclone	1776.22A	Volume (m^3)	[35]
	Fan	$900(A/300)^{0.25}$	Power (kW)	[34]
	Condenser	190 + 310A	Area (m^2)	
CO_2 storage system (CSS)	Compressor	$267{,}000(A/445)^{0.67}$	Power (kW)	[36]
	CO_2 tank	31.5 + 16A	Volume (L)	[34]
Direct cost	Installing	8 %A	TSA + ORC+EGC + CSS	[37]
	Instrumentation	5 %A		
	Piping	1.5 %A		
	Electric installing	1 %A		
Indirect cost	Engineering	7 %A	TSA + ORC+EGC + CSS + direct cost	[38,39]

Table 5
OPEX cost correlations and parameters.

Concept	Cost correlation	Parameters A, B, C, D, E, F and G	Ref.
Sorbent renovation	2 %A for PPN and MOF and 1 %A for AC	Total CAPEX	Own criterion
Increased fuel consumption	$\frac{3.6ABCD}{EFG}$	Power penalty (kW), CNG cost (€/kg), hour operation, operation days, LHV (kJ/kg), Combustion efficiency, engine efficiency	Own criterion
O&M	1 %A	Total CAPEX	[38,39]

device's parameter A is obtained from the simulations performed in the energy analysis [9].

Operating Expenditure (OPEX) constitutes the ongoing costs the CCS-ORC system incurs. The variables considered for the OPEX in this research are maintenance, sorbent renovation cost, and increased engine fuel consumption resulting from CCS-ORC system operation, as summarized in Table 5. The calculation of the latter is contingent upon the compressed natural gas (CNG) price, which is 1.017€/kg (average consumer price in Spain in March of 2024 tax included) [40,41], the power penalty over the engine provoked by the CCS-ORC system (PP), lower heating value (LHV), whose value is 48,351 kJ/kg [42], and the combustion and engine efficiencies of the average operational points of the engines within the WHTC. It also assumes vehicle operation of 350 days and 16 h per day. The values of all of these variables are listed in Appendix E.

3. CCS-ORC system concept design

The following subsections present the outcomes obtained based on the methodology previously outlined concerning the sizing of the heat exchangers, the design of the TSA device, and the calculation of the CAPEX and OPEX of the CCS-ORC system. These findings provide new insights into the sizing of a CCS-ORC system and techno-economic considerations of integrating this system in an HD-ICEV.

3.1. Heat exchanger sizing

Tables 6 and 7 list the results of the number and length of tubes and β for each heat exchanger, sorbent operating in the CCS-ORC system, and engine. These results are obtained by selecting two diameters of commercial copper tubes, 20 and 15 mm, intended for the heat exchangers of the CCS-ORC system that will be integrated into vehicles equipped with M936G and F1C engines, respectively.

These tables show that all heat exchangers' length restrictions were met. Consequently, many tubes are accommodated in the heat exchangers with more required area (HE-EG1. HE-EG2. ORC-C, ORC-E). As Fig. 5 shows, the lower the distance S_L, the greater the fluid speed and, therefore, the U value; this also allows greater compaction of the tubes and an increase in the β value. On the other hand, the heat exchangers of the CCS-ORC system operating with the F1C engine generally have a higher β than their counterpart, the M936G engine. This behaviour is caused by the

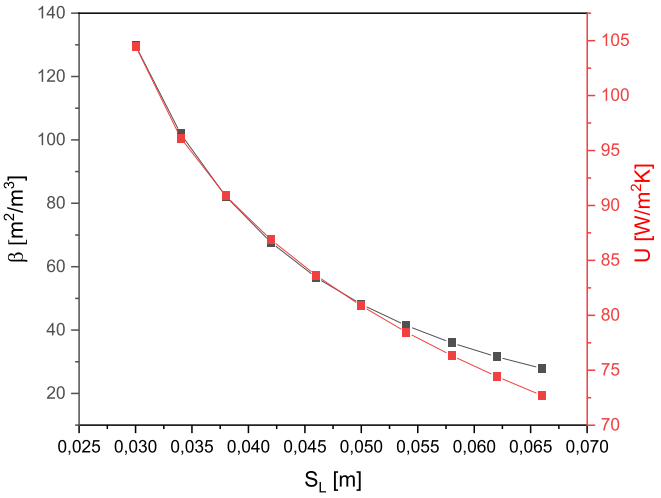

Fig. 5. β and U variation with the S_L distance in the heat exchanger arrangement

Table 6
β, number and length of tubes for the heat exchangers operating in the CCS-ORC system in the M936G engine.

Equipment	Number of tubes						Tube length [m]						β [m²/m³]					
	100 CCR			70 CCR			100 CCR			70 CCR			100 CCR			70 CCR		
	PPN	AC	MOF	PPN	AC	MOF	PPN	AC	MOF	PPN	AC	MOF	PPN	AC	MOF	PPN	AC	MOF
ORC-H	36			25			0.320	0.349	0.332	0.364	0.398	0.372	104.0	97.7	102.2	100.6		
ORC-E	256			256			0.472	0.446	0.477	0.508	0.494	0.508	124.5	123.7	124.5	124.9	124.5	124.6
ORC-C	375	372	420	450		480	0.584	0.598	0.592	0.585	0.591	0.593	107.0	99.3	125.2	115.2		106.9
HE-CO_2-C	28	36	16	25			0.543	0.463	0.498	0.425	0.466	0.424	97.2	93.5	97.9	97.3		
CO_2-Con	66	81	70	64			0.593	0.519	0.577	0.453	0.486	0.465	92.4	90.2	88.8	90.2	88.7	93.1
HE-EG1	675			510	480	496	0.597	0.597	0.598	0.585	0.596	0.589	126.6	114.6	116.0	102.3	109.4	132.7
HE-EG2	300		360	276	276	315	0.594	0.600	0.576	0.587	0.591	0.585	91.0	93.5	102.0	94.8	98.6	111.2

Table 7
β, number and length of tubes for the heat exchangers operating in the CCS-ORC system in the F1C engine.

Equipment	Number of tubes						Tube length [m]						β [m²/m³]					
	100 CCR			70 CCR			100 CCR			70 CCR			100 CCR			70 CCR		
	PPN	AC	MOF	PPN	AC	MOF	PPN	AC	MOF	PPN	AC	MOF	PPN	AC	MOF	PPN	AC	MOF
ORC-H	25			15	16		0.329	0.352	0.335	0.425	0.436	0.407	134.9	134.6		125.7	125.9	126.1
ORC-E	176	169	187	196			0.484	0.475	0.456	0.462	0.451	0.463	167.2	164.7	166.9	166.4	166.4	167.2
ORC-C	338	330	372	380		418	0.497	0.483	0.477	0.494	0.499	0.485	105	109	110.9	105.1	105.1	106.3
HE-CO_2-C	25			24*			0.423	0.465	0.423	0.385	0.423	0.384	101.6		100.2	141.4	145.1	141.4
CO_2-Con	64			49			0.431	0.459	0.441	0.414	0.444	0.424	98.1	96.2	99.36	100.1	102.7	104.1
HE-EG1	570	540	570	420	400	408	0.497	0.5	0.495	0.496	0.499	0.500	152.1	139.9	139.5	103.8	101.2	104.3
HE-EG2	276	260	300	240	250	260	0.492	0.489	0.487	0.487	0.460	0.499	109.2	110.3	107.9	124.9	126	121.7

* Calculated with a diameter of 12 mm.

lower mass flows of the substances that interact in the heat exchangers, which allows greater compaction of the tube bank arrangement and, therefore, an increase in the Reynolds number that allows compliance with the values of *U,* triggering higher values for *B* in the F1C engine.

It is important to note that the heat exchangers in the proposed CCS-ORC system's compaction level, with β values close to 100 m^2/m^3, is significant, as observed in [9]. However, there is still a considerable margin for improvement through a detailed design of heat exchangers, as these values are 4 times below the β value of compact heat exchange with phase change and 7 times below the β value of compact heat exchangers without phase change [43].

3.2. TSA device design

The transient state heat transfer mathematical model indicates that a duration of 180 s is suitable for the sorbent bed to attain the desired temperature at its centre. This short period of sorbent heating is due to the high temperature and velocity of the exhaust gases within the TSA device, which enhances the heat transfer parameters (*Re*, *h*), consequently diminishing the sorbent's heating time. This finding aligns with experimental results documented in the literature [44]. This time also allows a decrease in sorbent mass, therefore reducing the cost of the TSA device operation.

Tables 8 and 9 show the sizing obtained for the TSA device corresponding to each sorbent. As can be seen there, the TSA device attains its smallest size with the MOF sorbent, mainly because the MOF sorbent necessitates a lesser quantity of sorbent to capture an equivalent amount of CO_2 compared to the other sorbents. Moreover, the MOF sorbent has higher thermal conductivity when contrasted with the PPN and AC sorbents, facilitating the MOF sorbent in reaching the required desorption temperature more expeditiously. Consequently, the TSA device incorporating the MOF sorbent can accommodate a greater sorbent mass and, due to this, needs fewer tubes than the other TSA devices operating with the other sorbents.

Table 8
Sizing of the TSA device operating in the CCS-ORC system at 100 % of CCR.

Variable	M936G			F1C		
	AC	MOF	PPN	AC	MOF	PPN
Sorbent mass [kg]	17.03	8.09	9.56	8.44	4.01	4.73
Tube diameter [m]	0.078	0.122	0.09	0.046	0.09	0.062
Sorbent bed diameter [m]	0.074	0.118	0.086	0.042	0.086	0.058
Sorbent bed length [m]	6.95	1.62	4.08	10.69	1.51	4.45
Tube length [m]	1	1	1	1	1	1
Number of tubes	7	2	5	11	2	5
h [W/m^2K]	126.8	114.9	109.9	65.69	60.87	63.58
Re number	25,465	36,949	25,462	6337	12,967	8851
Shell diameter[m]	0.2496	0.2562	0.288	0.2024	0.189	0.1953
Heat transfer area [m^2]	1.72	0.77	1.41	1.59	0.57	0.97

Table 9
Sizing of the TSA device operating in the CCS-ORC system at 70 % of CCR.

Variable	M936G			F1C		
	AC	MOF	PPN	AC	MOF	PPN
Sorbent mass [kg]	11.92	5.66	6.69	5.91	2.81	3.31
Tube diameter [m]	0.092	0.142	0.106	0.064	0.114	0.082
Sorbent bed diameter [m]	0.088	0.138	0.102	0.06	0.11	0.078
Sorbent bed length [m]	3.44	0.83	2.03	3.67	0.65	1.72
Tube length [m]	0.90	0.90	0.90	0.70	0.70	0.70
Number of tubes	4	1	3	6	1	3
h [W/m^2K]	148.1	178.7	141.8	61.32	75.72	62.33
Re number	36,321	77,594	41,056	8385	22,016	11,665
Shell diameter[m]	0.2392	0.1704	0.2438	0.2048	0.1368	0.1886
Heat transfer area [m^2]	1.04	0.4	0.9	0.84	0.25	0.4

4. Tecno-economic assessment

4.1. CAPEX

Tables 10 and 11 show the values of parameter A, costs associated with individual devices, and the direct and indirect costs of CAPEX. As observed in these tables, no discernible impact exists on the CAPEX between different sorbents. Specifically, the CAPEX for the CCS-ORC system within the M936G engine at 100 % of CCR averages 68.17 k€, decreasing to 57.73 k€ at a 70 % CCR, denoting a reduction of 15.3 %. Similarly, in the F1C engine, the CAPEX at 100 % CCR stands at 39.92 k€, decreasing to 33.01 k€ at 70 % CCR, indicating a 17.3 % cost reduction. Notably, the disparity between sorbents at 100 % of CCR does not exceed 3.99 k€; at 70 % CCR, it remains within 2.7 k€ for both engines.

Fig. 6. shows the percentage weight in the CAPEX of each subsystem. The CSS system exerts the most significant influence on the CAPEX, constituting approximately 30 % of the initial investment, followed by the ORC system, which accounts for roughly 20 % of the initial investment at 100 % CCR. Notably, at 70 % CCR, an expected phenomenon unfolds: the CSS system reduces its weight over the total CAPEX while the ORC system increases its weight. This shift is attributed to the fact that it requires more robust equipment due to the high power production in this condition. Fig. 6 also shows that the TSA system with the MOF sorbent, for any engine and CCR, exhibits a weight in the CAPEX that is 40 % lower than with PPN and 60 % lower than with AC. However, the CAPEX of the ORC and EGC subsystems is higher with MOF compared to other sorbents. This, akin to the abovementioned observation, is attributed to the requirement for more robust equipment in MOF operation than other sorbents. The CCS subsystem in the M936G engine is directly correlated with the compression pressure of the compressor; hence, it manifests the following behaviour for this subsystem: PPN < AC < MOF. Nonetheless, MOF operation presents a higher value in the F1C engine at 100 % CCR due to the cumulative cost of heat exchangers and the compressor exceeding that of its AC operation counterpart.

The CAPEX obtained for the CCS-ORC systems is added to the initial purchase price of a CNG vehicle, allowing the increase in the initial purchase value of CNG vehicles that incorporate CCS-ORC systems to be calculated. The initial purchase values taken (baseline) are a bus of 75 m^3 and 19 t that uses the M936G engine [45] and a VAN of 5.2 t and 12 m^3 that uses the F1C engine [46]. Subsequently, these values are compared with other vehicles utilizing zero CO_2 emissions technologies, such as electric battery (EB) vehicles and those equipped with hydrogen-fuel-cell batteries (HFCB), as is shown in Table 12.

As can be seen in Table 12. vehicles that use zero-emission technologies are 61 % and 73 % more expensive than CNG vehicles without the CCS-ORC system (baseline). However, the CNG bus with the CCS-ORC system incorporated experiences only an increase of 18.2 % in its initial price for a 100 % CCR and 15.4 % for a 70 % CCR. On the other hand, installing the CCS-ORC system would increase its price to almost double the base case in the case of the VAN. The VAN with 100 % CCR turns out to be 33.2 % more expensive, and with 70 % CCR, it is 21.7 % more expensive than the EB VAN. These findings indicate that the initial cost is manageable for an owner in the case of the bus. Nevertheless, for smaller vehicles, the initial cost would not be feasible.

4.2. OPEX

Table 13 shows the OPEX results obtained for the four case studies. A

Table 10
CAPEX results of the CCS-ORC system operating in the M936G engine.

Process	Equipment	Parameter [A]						Cost [k€]					
		100 CCR			70 CCR			100 CCR			70 CCR		
		PPN	MOF	AC	PPN	MOF	AC	PPN	MOF	AC	PPN	MOF	AC
TSA	TSA-Device	1.41	0.77	1.72	0.9	0.4	1.04	4.56	2.71	5.42	3.10	1.54	3.51
Waste heat recovery (ORC)	ORC-expander	12.45	13.81	12.6	14.38	15.55	14.52	4.93	5.54	4.99	5.80	6.33	5.86
	ORC-pump	1.08	1.13	1	1.17	1.24	1.18	0.22	0.22	0.22	0.23	0.23	0.23
	ORC-C_5H_{10} tank	0.01	0.01	0.01	0.01	0.01	0.01	0.19	0.19	0.19	0.19	0.19	0.19
	ORC-Evaporator	7.59	7.66	7.17	8.16	8.17	7.95	2.54	2.56	2.41	2.72	2.72	2.65
	ORC-heater	0.72	0.75	0.79	0.57	0.59	0.63	0.41	0.42	0.43	0.37	0.37	0.39
	ORC-condenser	13.77	15.61	13.97	16.53	17.9	16.71	4.46	5.03	4.52	5.31	5.74	5.37
Exhaus gases condition	FG1	25.3	25.37	24.23	18.74	18.36	17.99	8.03	8.05	7.7	6.00	5.88	5.77
	FG2	11.2	13.02	11.31	10.18	11.58	10.25	3.66	4.23	3.7	3.35	3.78	3.37
	Cyclone	0.3	0.3	0.3	0.21	0.21	0.21	0.53	0.53	0.53	0.37	0.37	0.37
	Fan	0.99	0.7	1.05	1.282	0.834	1.35	0.22	0.2	0.22	0.23	0.21	0.23
CO_2 storage system	Condenser	2.46	2.54	2.64	1.82	1.87	1.96	0.95	0.98	1.01	0.75	0.77	0.80
	Cooling	0.95	0.75	1.05	0.67	0.67	0.73	0.48	0.42	0.52	0.40	0.40	0.42
	Compressor	17.93	18.33	21.76	12.7	13.03	15.28	11.64	11.86	13.65	8.78	8.96	10.21
	CO_2 tank	0.47	0.47	0.47	0.33	0.33	0.33	7.58	7.55	7.55	5.31	5.31	5.31
Direct cost	Installing	50.43	50.50	53.06	42.91	42.81	44.68	4.03	4.04	4.24	3.43	3.42	3.57
	Instrumentation							2.52	2.53	2.65	2.15	2.14	2.23
	Piping							0.76	0.76	0.8	0.64	0.64	0.67
	Electric installing							0.5	0.51	0.53	0.43	0.43	0.45
Indirect cost	Engineering	58.24	58.33	61.28	50.72	50.65	52.90	4.08	4.08	4.29	3.47	3.46	3.61
	Contingency							4.66	4.67	4.9	3.96	3.96	4.13
Total CAPEX								66.95	67.08	70.47	56.99	56.86	59.35

Table 11
CAPEX results of the CCS-ORC system operating in the F1C engine.

Process	Equipment	Parameter [A]						Cost [k€]					
		100 CCR			70 CCR			100 CCR			70 CCR		
		PPN	MOF	AC	PPN	MOF	AC	PPN	MOF	AC	PPN	MOF	AC
TSA	TSA-Device	0.97	0.57	1.59	0.54	0.25	0.84	3.31	2.09	5.06	2.00	1.03	2.92
Waste heat recovery (ORC)	ORC-expander	7.22	7.89	7.20	8.17	8.73	8.28	2.59	2.88	2.58	3.01	3.25	3.06
	ORC-pump	0.61	0.69	0.59	0.70	0.73	0.66	0.19	0.20	0.19	0.20	0.20	0.19
	ORC-C_5H_{10} tank	0.01	0.01	0.01	0.01	0.01	0.01	0.19	0.19	0.19	0.19	0.19	0.19
	ORC-Evaporator	4.01	4.02	3.79	4.27	4.27	4.16	1.43	1.44	1.36	1.51	1.51	1.48
	ORC-heater	0.39	0.39	0.42	0.30	0.31	0.33	0.31	0.31	0.32	0.28	0.29	0.29
	ORC-condenser	7.92	8.36	7.51	8.84	9.56	8.93	2.65	2.78	2.52	2.93	3.15	2.96
Exhaust gases condition (EGC)	FG1	13.34	13.30	12.72	9.81	9.61	9.41	4.33	4.31	4.13	3.23	3.17	3.11
	FG2	6.40	6.88	5.99	5.38	6.12	5.42	2.17	2.32	2.05	1.86	2.09	1.87
	Cyclone	0.15	0.15	0.15	0.11	0.11	0.11	0.27	0.27	0.27	0.19	0.19	0.19
	Fan	0.46	0.32	0.48	0.31	0.23	0.32	0.18	0.16	0.18	0.16	0.15	0.16
CO_2 storage system (CSS)	Condenser	1.30	1.33	1.38	0.96	0.98	1.02	0.59	0.60	0.62	0.49	0.49	0.51
	Cooling	0.50	0.50	0.55	0.35	0.35	0.38	0.35	0.35	0.36	0.30	0.30	0.31
	Compressor	9.71	9.92	11.78	6.88	7.03	8.34	7.04	7.17	8.25	5.31	5.40	6.22
	CO_2 tank	0.24	0.24	0.24	0.17	0.17	0.17	3.81	3.81	3.81	2.67	2.67	2.67
Direct cost	Installing	29.40	28.88	31.89	24.33	24.09	26.13	2.35	2.31	2.55	1.95	1.93	2.09
	Instrumentation							1.47	1.44	1.59	1.22	1.20	1.31
	Piping							0.44	0.43	0.48	0.36	0.36	0.39
	Electric installing							0.29	0.29	0.32	0.24	0.24	0.26
Indirect cost	Engineering	34	33.4	36.8	28.88	28.57	31.07	2.38	2.34	2.58	1.97	1.95	2.11
	Contingency							2.72	2.67	2.95	2.25	2.23	2.41
Total CAPEX								39.05	38.36	42.35	32.31	32.00	34.71

vehicle yearly operation of 350 days and 16 h per day is considered. The OPEX of the CCS-ORS system calculated for the M936G engine, at 100 % of CCR, is on average 10.91 k€ and 4.4 k€ for 70 % of CCR, and the F1C engine is 6.05 and 2.24 k€ for 100 and 70 % of CCR, respectively. Likewise, it is observed that although the AC has a 50 % lower sorbent renewal cost in the OPEX calculation because it is a commercial material, the operating expenses of the CCS-ORC system obtained in the two engines with AC are, on average, 27 % and 43 % higher than 100 % and 70 % CCR, respectively, compared to the OPEX values obtained with MOF. This behaviour is due to the greater penalty that the CCS-ORC system exerts on engines with AC operation, which increases fuel consumption.

4.3. Payback analysis

As observed in the results found, the initial cost of installing a CCS-ORC system operating in a vehicle with an M936G engine is between 15 and 18 % (depending on the capture rate), and in a vehicle with an F1C engine, the cost of the vehicle increases to almost double. Furthermore, both vehicles' average annual operational expenses are 15 and 7 % of the initial CCS-ORC system cost for 100 and 70 % CCR, respectively. These results suggest that integrating a CCS-ORC system into heavy-duty vehicles may lack economic feasibility unless accompanying benefits or exemptions from avoiding emissions-related taxes exist. Hence, this section will undertake an economic assessment as an entry point from 2027. when a package of stricter rules comes into force to reduce transport sector emissions through a specialized emission

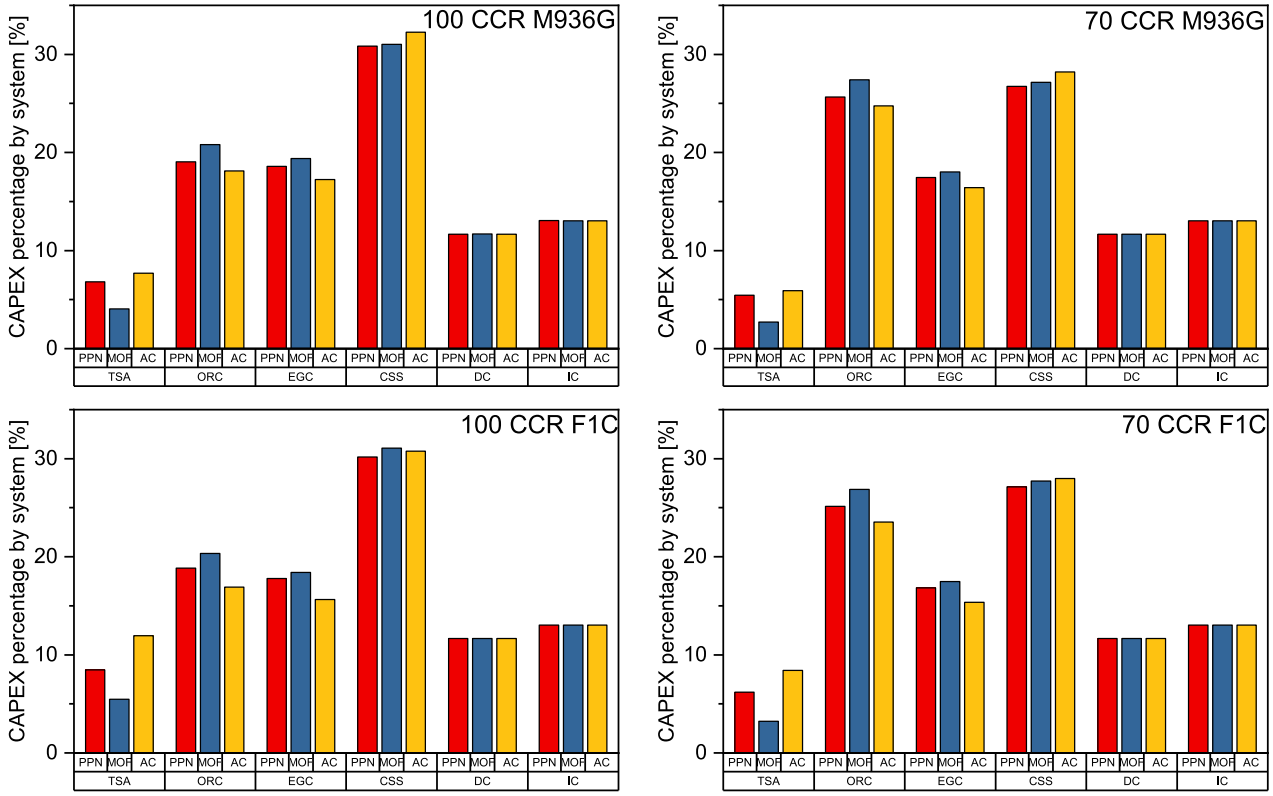

Fig. 6. CAPEX percentage by sub-system in the CCS-ORC system.

Table 12
CAPEX including the initial purchase of the vehicle.

Vehicle	Technology	Purchase [k€]	Difference from baseline [%]	Reference
Bus with a M936G engine (or similar V_d) and useful space of 75 m^3	CNG	374.6	0.0	[47,48]
	HFCB	650	−73.5	[49]
	EB	604	−61.2	[50]
	CNG + CCS-ORC at 100 % of CCR	442.	−18.2	Own study
	CNG + CCS-ORC at 70 % of CCR	432.3	−15.4	Own Study
VAN with a F1C engine (or similar V_d) and useful space of 12 m^3	CNG	40	0.0	[51]
	EB	60	50.0	[52,53]
	CNG + CCS-ORC at 100 % of CCR	79.9	−99.8	Own study
	CNG + CCS-ORC at 70 % of CCR	73	−82.5	Own Study

trading system often referred to as 'ETS2' [54]. In this, the European Union established the charge for CO_2 emission rights to the transport sector with an initial value of 45 €/tCO_2 [54,55]. This will increase the cost of goods transported if the transport sector does not have a broader range of technologies to reduce its CO_2 emissions by that date.

The initial analysis will determine the payback time for a CCS-ORC system integrated into a heavy-duty vehicle. Initially, the annual CO_2 emissions avoided for each engine are obtained utilizing the data provided in section 2.4. This data is multiplied by the established price of the CO_2 emission rights; thereby, the income is obtained for each case. Table 14 shows the values obtained from the income and the annual net profit, which is the difference between the OPEX and the income. Finally, the payback time of the CCS-ORC system is determined by calculating the net present value (NPV) using Eq. 22. In this calculation, i represents the interest rate, set at 4 %, t denotes the number of years, and n signifies a heavy transport vehicle's lifespan, typically 10 years, according to the literature [56]. Fig. 7 provides the result obtained for the NPV.

$$NPV = \sum_{t=0}^{n} \frac{Profits_t}{(1+i)^t} - CAPEX \tag{22}$$

Table 13
OPEX for the CCS-ORC systems.

Concept	M936G						F1C					
	100 CCR			70 CCR			100 CCR			70 CCR		
	PPN	MOF	AC	PPN	MOF	AC	PPN	MOF	AC	PPN	MOF	AC
Sorbent renovation [k€/year]	1.34	1.34	0.70	0.85	0.85	0.59	0.59	0.58	0.42	0.48	0.48	0.35
Fuel consumption increase [k€/year]	8.39	7.51	11.40	2.53	2.01	4.63	4.69	4.18	6.49	1.16	0.86	2.42
O&M [k€/year]	0.67	0.67	0.7	0.57	0.57	0.59	0.39	0.38	0.38	0.32	0.32	0.35
Total OPEX [k€/year]	10.40	9.52	12.81	3.95	3.43	5.82	5.66	5.14	7.33	1.97	1.66	3.11

Table 14
Incomes and Profits obtained for integrating a CCS-ORC system in a heavy-duty vehicle.

	M936G						F1C					
Concept	100			70			100			70		
	PPN	MOF	AC	PPN	MOF	AC	PPN	MOF	AC	PPN	MOF	AC
OPEX [k€/year]	10.40	9.52	12.81	3.95	3.43	5.82	5.66	5.14	7.33	1.97	1.66	3.11
Income [k€/year]	11.33			7.93			5.67			3.97		
Profits [k€/year]	0.93	1.81	−1.48	3.98	4.50	2.11	0.01	0.53	−1.66	2.00	2.31	0.86

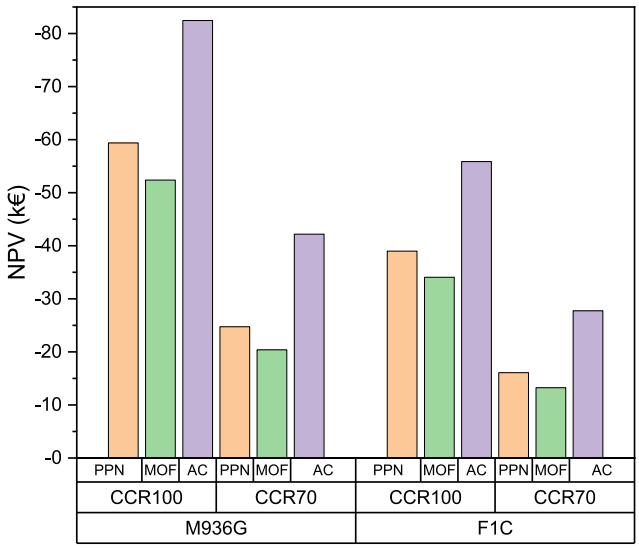

Fig. 7. NPV calculated at 10 years of CCS-ORC system for the whole sorbent, CCR and engines.

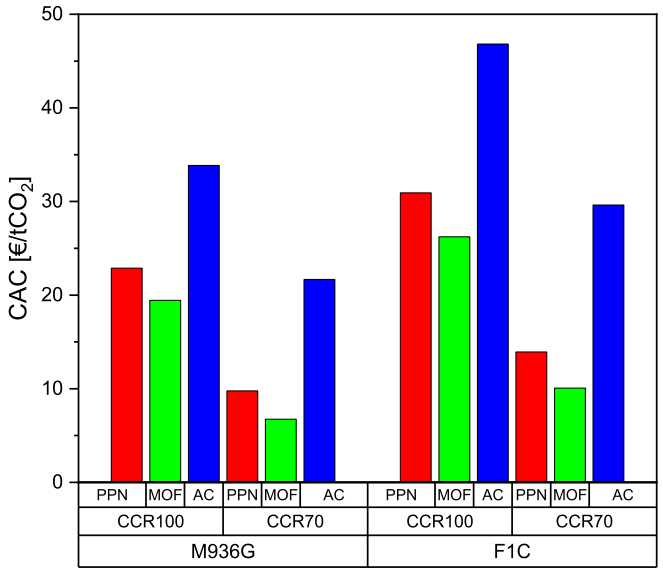

Fig. 8. CAC calculated of CCS-ORC system for the whole sorbent, CCR and engines.

The values obtained from the payback time indicate that the capital expenditures (CAPEX, see Tables 10 and 11) fails to be recouped with any sorbent and with any under CCR conditions over the vehicles' useful lifespan. Notably, even with the AC in both engines and at 100 % of CCR, a reduction in CAPEX is not achieved. This behaviour is attributed to the fact that, under this CCR condition in both motors, no profits are obtained with the AC, but, on the contrary, additional expenses are incurred for the operation of the CCS-ORC system.

Conversely, with the other two sorbents at 100 % CCR, a partial recovery of the initial investment is achieved. Specifically, with MOF, the recovery percentages stand at 22 and 64 % at 100 and 70 % CCR, respectively, in the M936G engine, and 11 and 59 % at 100 and 70 % CCR, respectively, in the F1C engine. Employing PPN yields recovery percentages of 11 % and 57 % at 100 % and 70 % CCR, respectively, for the M936G engine and 50 % at 70 % CCR for the F1C engine.

As evidenced in the data previously shown, there is a more significant recovery on the initial investment of the CCS-ORC system in the M936G engine, especially at 70 % CCR, due to the lower initial investment and the more significant amount of CO_2 captured, which translates into a higher annual benefit compared to the operation of the CCS-ORC system in the vehicle with an F1C engine.

Despite not achieving the recovery of the investment within the established lifespan vehicle period, it is relevant to note that the carbon abatement costs (CAC) (calculated using Eq. 23) obtained for the CCS-ORC systems proposed in this research, operating at 100 % CCR, vary from 19.4 €/tCO_2 with MOF up to 33.9 €/tCO_2 with AC in the vehicle equipped with the M936G engine, and from 26.2 €/tCO_2 with MOF to 46.8 €/tCO_2 in the vehicle with the F1C engine, as shown in Fig. 8. These values are below those observed in other industries, such as glass and steel, whose CCS costs range between 50 and 350 €/tCO_2 [57,58]. As expected, Fig. 8 shows a decrease in CAC with the CCR reduction due to the CCS-ORC system's lower CAPEX. Furthermore, a higher CAC is seen in both CCRs in the vehicle equipped with the F1C engine, which is attributed to the lower benefit obtained from the CCS-ORC system operating in this vehicle.

$$CAC = \frac{\frac{CAPEX}{lifespan} - Profits}{\frac{tCO_2}{year}_{avoided}} \quad (23)$$

5. Sensitivity analysis

This section introduces two sensitivity analyses. The first seeks to establish the appropriate price of the CO_2 emissions tax to achieve the payback on the initial investment within the operational lifespan of a heavy-duty work vehicle (10 years). The second aims to identify the engine size (by varying the engine displacement volume) that achieves a CAC of zero. This latter analysis is made in the same period, and the price of the CO_2 emission tax remains fixed at 45 €/tCO_2.

Fig. 9 shows the results of the first analysis. It discloses that, to achieve a 10-year payback on investment with a CCR of 100 %, the required CO_2 emission rights prices are 70.6. 74.4 and 85.4 €/tCO_2 for the MOF sorbents, PPN and AC, respectively, in the M936G engine and the F1C engine, the value of the tax with MOF, PPN and AC must be 78.3. 83.8 and 99.7 €/tCO_2. respectively. On the other hand, by reducing the CCR to 70 %, a decrease is observed in the required value of the CO_2 tax to achieve the payback of the initial investment in the established period. Compared to the 100 % CCR scenario, this reduction amounts to 10 and 15 €/tCO_2 for all three sorbents in the M936G and F1C engines, respectively. Notably, the analysis indicates that smaller vehicles necessitate higher CO_2 tax payments to achieve the desired return on investment within the designated timeframe.

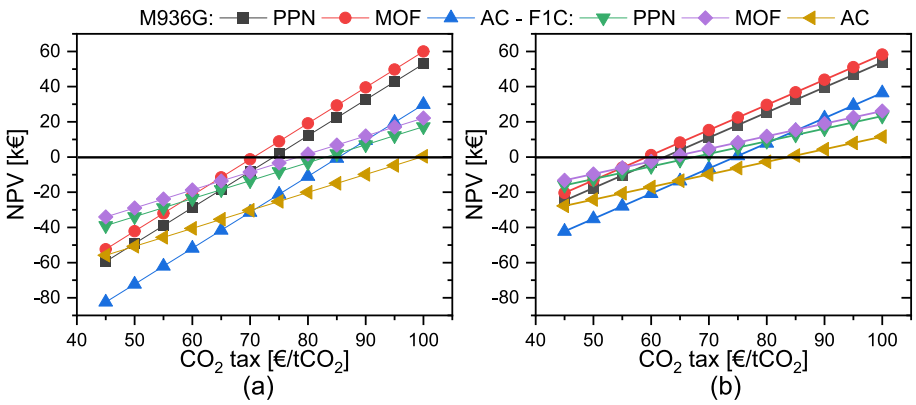

Fig. 9. Payback sensitivity analysis: a) 100 CCR and b) 70 CCR.

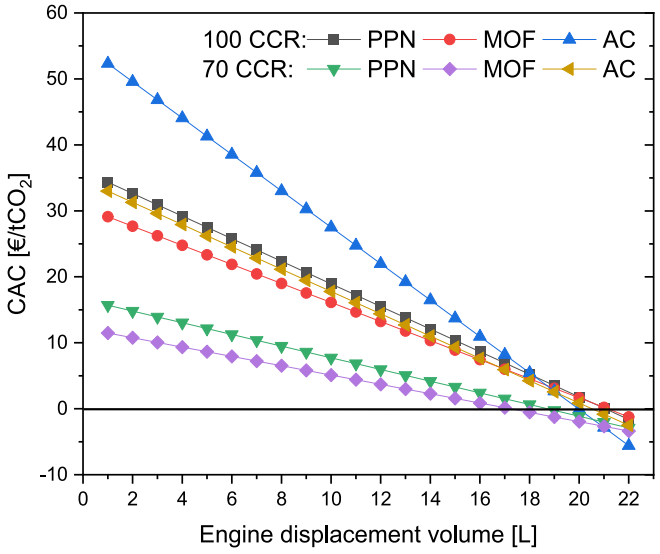

Fig. 10. CAC sensitivity analysis for engine size.

Fig. 10 reveals that achieving a CAC of zero or less at 100 %, CCR requires an engine with a displacement volume (V_d) greater than 20 L with AC and 22 L with MOF and PPN. This specific finding is attributed to the steeper negative slope of the CAC of the CCS-ORC system between the F1C and M936G engines with AC. On the other hand, when moving to the CCR of 70 %, it is observed that the CAC of zero or less is obtained with a V_d of 18 L with MOF, 19 L with PPN and 21 L with AC. Although AC exhibits a higher negative slope in the latter scenario compared to other sorbents, this result aligns more closely with the trend observed in the preceding findings. Finally, regardless of the CCR rate, it is evident that a CCS-ORC system could yield a CAC of zero in engines with high V_d.

6. Conclusions

The present work constitutes the first sizing and techno-economic analysis of a CCS-ORC integrated into a heavy-duty vehicle. The CCS-ORC takes advantage of the waste heat in the exhaust gases to perform the TSA stages. Additionally, it integrates an ORC cycle to supply the power demand of the CO_2 compression stage. This is evaluated with two CCRs and three sorbents in two engines with different engine volume displacements. The heat exchangers and TSA device required for the correct operation of the CCS-ORC system are sizing, searching for the maximum compaction possible. A techno-economic analysis is conducted to determine the initial expenses of an HD-ICEV with an integrated CCS-ORC system and the operational cost of the latter. Finally, the economic feasibility of this integration, under the scenario when the transport sector must pay for the CO_2 emissions rights, is evaluated.

The outcomes of the concept design conducted in the present research show that the volumes found for the TSA device, whose highest value is scarcely 0.26 m^3, and the achieved compaction levels in the heat exchangers of the CCS-ORC system suggest that the CCS-ORC system can be installed in an HD-ICEV with minimal impact on the useful space. Nevertheless, in future research endeavours, a detailed design of the heat exchangers could achieve higher β values. This improvement would enhance the compaction of the CCS-ORC system, facilitating its integration into the HD-ICEV. Although, this does not mean a reduction in the cost since it is calculated with the heat exchanger area.

On the other hand, the CAPEX results show that the increase in the initial investment of a large vehicle with an integrated CCS-ORC system is barely higher than the baseline vehicle. Conversely, it is much lower than the initial investment for other zero-emissions technologies. It should be noted that the techno-economic analyses indicate that integrating a CCS-ORC system in a vehicle with a small engine is not feasible.

Although the NPV in the lifespan of a heavy-duty vehicle is far from zero, values between 19 and 47 €/tCO_2 of carbon abatement cost at 100 % CCR are obtained, which are low compared to other industries. So, the transport sector could incur this investment if it aims to meet the CO_2 reduction objectives established by the European Union for the year 2050. The payback of the initial investment can even be achieved with a CO_2 tax greater than 65 €/tCO_2. The captured CO_2 could even be sold as raw material for producing e-fuels, which would compensate for the vehicle's operating cost and provide additional income that would increase the benefits obtained by integrating a CCS-ORC system. The captured CO_2 is also prevented from being stored underground, thus giving the CO_2 a productive value.

To sum up, this study shows that integrating the CCS-ORC system in vehicles used in heavy-duty transport is promising from the CO_2 mitigation perspective and a medium-term economic point of view. The proposed integration avoids the increase of CO_2 in the atmosphere provoked by the transport sector and provides CO_2 as raw material for manufacturing e-fuels. For this reason, future endeavours should encompass studies about life cycle assessments to determine the environmental and social impacts and experimental studies to validate the CCS-ORC system under actual conditions. In this way, the knowledge gap is closed, and thus, contributes to the development of a novel application that allows complete decarbonization of this energy-intensive sector.

CRediT authorship contribution statement

Alexander García-Mariaca: Writing – review & editing, Writing – original draft, Software, Methodology, Formal analysis, Data curation, Conceptualization. **Eva Llera-Sastresa:** Writing – review & editing, Project administration, Methodology, Investigation, Funding

acquisition, Formal analysis, Conceptualization.

Declaration of competing interest

None.

Data availability

Data will be made available on request.

Acknowledgements

This paper is part of the R&D project PID2021-125137OB-I00, funded by MCIN/ AEI /10.13039/501100011033/ and by "ERDF A way of making Europe".

Appendix A. Appendix

Area, temperature, pressure and mass flows of each heat exchanger with the CCS-ORC system operating with PPN.

Engine	CCR	Heat exchanger	Area [m^2]	$\dot{m}_{in\_HF}$ [kg/h]	T_{in_HF} [°C]	T_{out_HF} [°C]	$\dot{m}_{in\_CF}$ [kg/h]	T_{in_CF} [°C]	T_{out_CF} [°C]	P_{in_HF} [bar]	P_{out_HF} [bar]	P_{in_CF} [bar]	P_{out_CF} [bar]
		ORC-H	0.72	104.60	573.87	119.49	527.52	50.93	99.49	75	75	24.9	22.9
		ORC-E	7.59	681.48	421.73	119.49	527.52	99.49	184.15	1.09	1.09	22.9	20.9
		ORC-C	13.77	527.52	121.02	48.87	43,529.61	30.00	35.99	1.5	1	1	1
M936G	100	HE-CO_2-C	0.95	104.60	150.00	39.23	43,529.61	35.99	36.23	1	1	1	1
		CO_2-Con	2.46	104.60	119.49	29.30	43,529.61	25.00	25.58	75	75	1	1
		HE-EG1	25.30	681.48	119.49	39.23	43,529.61	36.23	41.05	1	1	1	1
		HE-EG2	11.20	681.48	39.23	30.00	43,529.61	25.58	26.31	1	1	1	1
		ORC-H	0.57	73.53	581.23	102.28	617.26	50.93	82.47	75	75	24.9	22.9
		ORC-E	8.16	681.48	483.01	102.47	617.26	82.47	184.15	1.09	1.09	22.9	20.9
		ORC-C	16.53	617.26	121.07	48.87	32,357.23	30.00	39.42	1.5	1	1	1
M936G	70	HE-CO_2-C	0.67	73.53	150.00	42.70	32,357.23	39.42	39.65	1	1	1	1
		CO_2-Con	1.82	73.53	102.28	29.30	32,357.23	25.00	25.50	75	75	1	1
		HE-EG1	18.74	477.04	102.47	42.65	32,357.23	39.65	43.55	1	1	1	1
		HE-EG2	10.18	477.04	42.65	30.00	32,357.23	25.50	26.52	1	1	1	1
		ORC-H	0.39	42.49	573.36	79.39	203.44	38.80	95.97	75	75	24.9	22.9
		ORC-E	4.01	276.75	408.58	115.97	203.44	95.97	184.15	1.09	1.09	22.9	20.9
		ORC-C	7.92	203.44	121.05	36.76	17,615.38	30.00	35.98	1.5	1	1	1
F1C	100	HE-CO_2-C	0.50	42.49	150.00	38.98	17,615.38	35.98	36.22	1	1	1	1
		CO_2-Con	1.30	42.49	79.39	29.30	17,615.38	25.00	25.46	75	75	1	1
		HE-EG1	13.34	276.75	115.97	39.22	17,615.38	36.22	41.00	1	1	1	1
		HE-EG2	6.40	276.75	39.22	30.00	17,615.38	25.46	26.29	1	1	1	1
		ORC-H	0.30	29.83	580.19	72.21	239.41	40.53	76.58	75	75	24.9	22.9
		ORC-E	4.27	276.75	470.12	96.58	239.41	76.58	184.15	1.09	1.09	22.9	20.9
		ORC-C	8.84	239.41	121.03	38.48	13,162.36	30.00	39.36	1.5	1	1	1
F1C	70	HE-CO_2-C	0.35	29.83	150.00	42.36	13,162.36	39.36	39.58	1	1	1	1
		CO_2-Con	0.96	29.83	72.21	29.30	13,162.36	25.00	25.41	75	75	1	1
		HE-EG1	9.81	193.73	96.58	42.58	13,162.36	39.58	43.38	1	1	1	1
		HE-EG2	5.38	193.73	42.58	30.00	13,162.36	25.41	26.53	1	1	1	1

Appendix B. Appendix

Area, temperature, pressure and mass flows of each heat exchanger with the CCS-ORC system operating with MOF.

Engine	CCR	Heat exchanger	Area [m^2]	$\dot{m}_{in\_HF}$ [kg/h]	T_{in_HF} [°C]	T_{out_HF} [°C]	$\dot{m}_{in\_CF}$ [kg/h]	T_{in_CF} [°C]	T_{out_CF} [°C]	P_{in_HF} [bar]	P_{out_HF} [bar]	P_{in_CF} [bar]	P_{out_CF} [bar]
		ORC-H	0.75	104.99	584.02	116.12	591.17	50.93	96.11	77.9	77.9	24.9	22.9
		ORC-E	7.66	681.48	458.93	116.13	591.17	96.11	184.15	1.09	1.09	22.9	20.9
		ORC-C	15.61	591.17	121.02	48.87	38,743.25	30.00	37.54	1.5	1	1	1
M936G	100	HE-CO_2-C	0.95	104.99	150.00	40.80	38,743.25	37.54	37.81	1	1	1	1
		CO_2-Con	2.54	104.99	116.12	29.30	38,743.25	25.00	25.66	77.9	77.9	1	1
		HE-EG1	25.37	681.48	116.13	40.81	38,743.25	37.81	42.97	1	1	1	1
		HE-EG2	13.02	681.48	40.81	30.00	38,743.25	25.66	26.66	1	1	1	1
		ORC-H	0.59	73.67	591.15	101.33	659.74	50.93	81.33	77.9	77.9	24.9	22.9
		ORC-E	8.17	681.48	508.67	101.33	659.74	81.33	184.15	1.09	1.09	22.9	20.9
		ORC-C	17.90	659.74	121.02	48.87	29,315.32	30.00	41.12	1.5	1	1	1
M936G	70	HE-CO_2-C	0.67	73.67	150.00	44.35	29,315.32	41.12	41.36	1	1	1	1
		CO_2-Con	1.87	73.67	101.33	29.30	29,315.32	25.00	25.56	77.9	77.9	1	1
		HE-EG1	18.36	477.04	101.33	44.36	29,315.32	41.36	45.42	1	1	1	1
		HE-EG2	11.58	477.04	44.36	30.00	29,315.32	25.56	26.91	1	1	1	1
F1C	100	ORC-H	0.39	42.64	603.38	78.40	229.23	40.49	92.90	77.9	77.9	24.9	22.9

(continued on next page)

(*continued*)

Engine	CCR	Heat exchanger	Area [m^2]	$\dot{m}_{in\_HF}$ [kg/h]	T_{in_HF} [°C]	T_{out_HF} [°C]	$\dot{m}_{in\_CF}$ [kg/h]	T_{in_CF} [°C]	T_{out_CF} [°C]	P_{in_HF} [bar]	P_{out_HF} [bar]	P_{in_CF} [bar]	P_{out_CF} [bar]
		ORC-E	4.02	276.75	445.94	112.90	229.23	92.90	184.15	1.09	1.09	22.9	20.9
		ORC-C	8.36	229.23	121.03	38.44	15,659.74	30.00	37.53	1.5	1	1	1
		HE-CO_2-C	0.50	42.64	150.00	40.53	15,659.74	37.53	37.80	1	1	1	1
		CO_2-Con	1.33	42.64	78.40	29.30	15,659.74	25.00	25.52	77.9	77.9	1	1
		HE-EG1	13.30	276.75	112.90	40.81	15,659.74	37.80	42.93	1	1	1	1
		HE-EG2	6.88	276.75	40.81	30.00	15,659.74	25.52	26.64	1	1	1	1
		ORC-H	0.31	29.92	590.55	71.49	256.24	40.64	75.40	77.9	77.9	24.9	22.9
		ORC-E	4.27	276.75	495.89	95.40	256.24	75.40	184.15	1.09	1.09	22.9	20.9
		ORC-C	9.56	256.24	121.04	38.59	11,909.73	30.00	41.06	1.5	1	1	1
F1C	70	HE-CO_2-C	0.35	29.92	150.00	44.06	11,909.73	41.06	41.31	1	1	1	1
		CO_2-Con	0.98	29.92	71.49	29.30	11,909.73	25.00	25.46	77.9	77.9	1	1
		HE-EG1	9.61	193.73	95.40	44.31	11,909.73	41.31	45.27	1	1	1	1
		HE-EG2	6.12	193.73	44.31	30.00	11,909.73	25.46	26.91	1	1	1	1

Appendix C. Appendix

Area, temperature, pressure and mass flows of each heat exchanger with the CCS-ORC system operating with AC.

Engine	CCR	Heat exchanger	Area [m^2]	$\dot{m}_{in\_HF}$ [kg/h]	T_{in_HF} [°C]	T_{out_HF} [°C]	$\dot{m}_{in\_CF}$ [kg/h]	T_{in_CF} [°C]	T_{out_CF} [°C]	P_{in_HF} [bar]	P_{out_HF} [bar]	P_{in_CF} [bar]	P_{out_CF} [bar]
		ORC-H	0.79	113.81	625.81	127.79	535.11	50.93	107.78	85.73	85.73	24.9	22.9
		ORC-E	7.17	681.48	421.58	127.91	535.11	107.78	184.15	1.09	1.09	22.9	20.9
		ORC-C	13.97	535.11	121.02	48.87	44,269.95	30.00	35.97	1.5	1	1	1
M936G	100	HE-CO_2-C	1.05	113.81	150.00	39.24	44,269.95	35.97	36.24	1	1	1	1
		CO_2-Con	2.64	113.81	127.79	29.30	44,269.95	25.00	25.65	85.73	85.73	1	1
		HE-EG1	24.23	681.48	127.91	39.24	44,269.95	36.24	41.12	1	1	1	1
		HE-EG2	11.31	681.48	39.24	30.00	44,269.95	25.65	26.37	1	1	1	1
		ORC-H	0.63	79.90	633.15	108.01	623.90	50.93	88.02	85.73	85.73	24.9	22.9
		ORC-E	7.95	681.48	482.90	108.02	623.90	88.02	184.15	1.09	1.09	22.9	20.9
		ORC-C	16.71	623.90	121.02	48.87	32,794.40	30.00	39.40	1.5	1	1	1
M936G	70	HE-CO_2-C	0.73	79.90	149.98	42.65	32,794.40	39.40	39.64	1	1	1	1
		CO_2-Con	1.96	79.90	108.01	29.30	32,794.40	25.00	25.55	85.73	85.73	1	1
		HE-EG1	17.99	477.04	108.02	42.64	32,794.40	39.64	43.58	1	1	1	1
		HE-EG2	10.25	477.04	42.64	30.00	32,794.40	25.55	26.57	1	1	1	1
		ORC-H	0.42	46.22	625.21	87.26	206.70	40.30	106.17	85.73	85.73	24.9	22.9
		ORC-E	3.79	276.75	408.42	126.17	206.70	106.17	184.15	1.09	1.09	22.9	20.9
		ORC-C	7.51	206.70	121.05	38.26	17,843.54	30.00	35.96	1.5	1	1	1
F1C	100	HE-CO_2-C	0.55	46.22	150.00	38.96	17,843.54	35.96	36.23	1	1	1	1
		CO_2-Con	1.38	46.22	87.26	29.30	17,843.54	25.00	25.52	85.73	85.73	1	1
		HE-EG1	12.72	276.75	126.17	39.23	17,843.54	36.23	41.13	1	1	1	1
		HE-EG2	5.99	276.75	39.23	30.00	17,843.54	25.52	26.34	1	1	1	1
		ORC-H	0.33	32.45	632.61	71.79	242.05	40.57	83.19	85.73	85.73	24.9	22.9
		ORC-E	4.16	276.75	470.00	103.19	242.05	83.19	184.15	1.09	1.09	22.9	20.9
		ORC-C	8.93	242.05	121.04	38.52	13,247.07	30.00	39.40	1.5	1	1	1
F1C	70	HE-CO_2-C	0.38	32.45	150.00	42.40	13,247.07	39.40	39.64	1	1	1	1
		CO_2-Con	1.02	32.45	71.79	29.30	13,247.07	25.00	25.43	85.73	85.73	1	1
		HE-EG1	9.41	193.73	103.19	42.64	13,247.07	39.64	43.53	1	1	1	1
		HE-EG2	5.42	193.73	42.64	30	13,247.07	25.43	26.55	1	1	1	1

Appendix D. Appendix

Discretization of the mathematical model used in the design of the TSA device:

Central nodes

$$k\frac{T_{m+1}^{i+1}-2T_m^{i+1}+T_{m-1}^{i+1}}{\Delta r^2}+\frac{k}{i}\left(\frac{T_{m+1}^{i+1}-T_{m-1}^{i+1}}{2\Delta r^2}\right)=\rho C_p{}_i\frac{T_m^{i+1}-T_m^i}{\Delta t}$$

At $r=0$ Eq. 14 is indeterminate, therefore the l'Hôpital's rule must be applied, obtaining:

$$2k\frac{\partial^2 T}{\partial r^2}=\rho C_p\frac{\partial T}{\partial t}$$

This latter equation is discretized by taking the mirror image and isolated boundary, obtaining the following discretization:

$$4k\frac{T_{m+1}^{i+1}-T_m^{i+1}}{\Delta r^2}=\rho C_p{}_i\frac{T_m^{i+1}-T_m^i}{\Delta t}$$

On the surface

$$\frac{2kT_{m-1}^{i+1}}{dr^2} - T_m^{i+1}\left[\left(\frac{2k}{dr^2}+\frac{2h}{dr}+\frac{2h}{idr}+\frac{\rho Cp}{\Delta t}\right)+1\right] = -T_m^i\left(\frac{\rho Cp}{\Delta t}\right) - \frac{2hT_\infty}{dr} - \frac{hT_\infty}{idr}$$

Appendix E. Appendix

Combustion and engine efficiencies at 1300 rpm and 25 of EL for the M936G engine and at 2000 rpm and 25 of EL for the F1C engine.

Engine	M936G	F1C
Engine efficiency (η_{eng}) [%]	20.65	17.05
Combustion efficiency (η_{com}) [%]	98.71	98.14

References

[1] Bains P, Psarras P, Wilcox J. CO 2 capture from the industry sector. Prog Energy Combust Sci 2017;63:146–72. https://doi.org/10.1016/j.pecs.2017.07.001.
[2] International Energy agency. Global energy-related CO2 emissions by sector –Charts – Data & Statistics - IEA. https://www.iea.org/reports/co2-emissions-in-2022; 2022 (accessed February 28, 2023).
[3] Voice A, Hamad E. Mobile carbon capture for long-haul commercial transport: design. Integr Res SSRN Electron J 2022. https://doi.org/10.2139/ssrn.4280720.
[4] García-Mariaca A, Llera-Sastresa E. Energy and economic analysis feasibility of CO2 capture on a natural gas internal combustion engine. Greenh Gas Sci Technol 2022. https://doi.org/10.1002/GHG.2176.
[5] Kim J, Yoo Y, Kim S, Beak J, Oh S-D, Lee J, et al. Design and assessment of a novel mobile carbon capture system: energy and exergy analyses. Energ Conver Manage 2024;300:117934. https://doi.org/10.1016/j.enconman.2023.117934.
[6] Sharma S, Maréchal F. Carbon dioxide capture from internal combustion engine exhaust using temperature swing adsorption. Front Energy Res 2019;7:1–12. https://doi.org/10.3389/fenrg.2019.00143.
[7] García-Mariaca A, Llera-Sastresa E. Review on carbon capture in ICE driven transport. Energies (Basel) 2021;14:6865. https://doi.org/10.3390/en14216865.
[8] García-Mariaca A, Llera-Sastresa E, Moreno F. Application of ORC to reduce the energy penalty of carbon capture in non-stationary ICE. Energ Conver Manage 2022;268:116029. https://doi.org/10.1016/J.ENCONMAN.2022.116029.
[9] García-Mariaca A, Llera-Sastresa E, Moreno F. CO2 capture feasibility by temperature swing adsorption in heavy-duty engines from an energy perspective. Energy 2024;292:130511. https://doi.org/10.1016/j.energy.2024.130511.
[10] Invernizzi CM, Iora P, Manzolini G, Lasala S. Thermal stability of n-pentane, cyclopentane and toluene as working fluids in organic Rankine engines. Appl Therm Eng 2017;121:172–9. https://doi.org/10.1016/j.applthermaleng.2017.04.038.
[11] Shu G, Li X, Tian H, Liang X, Wei H, Wang X. Alkanes as working fluids for high-temperature exhaust heat recovery of diesel engine using organic Rankine cycle. Appl Energy 2014;119:204–17. https://doi.org/10.1016/j.apenergy.2013.12.056.
[12] Verdegaal WM, Wang K, Sculley JP, Wriedt M, Zhou HC. Evaluation of metal-organic frameworks and porous polymer networks for CO2-capture applications. ChemSusChem 2016;9:636–43. https://doi.org/10.1002/cssc.201501464.
[13] Plaza MG, García S, Rubiera F, Pis JJ, Pevida C. Post-combustion CO2 capture with a commercial activated carbon: comparison of different regeneration strategies. Chem Eng J 2010;163:41–7. https://doi.org/10.1016/j.cej.2010.07.030.
[14] Žukauskas A. Heat transfer from tubes in crossflow. Adv Heat Transf 1972;8:93–160. https://doi.org/10.1016/S0065-2717(08)70038-8.
[15] Gnielinski V. New equations for heat and mass transfer in turbulent pipe and channel flow. Int Chem Eng 1976;16:359–67.
[16] Gu HF, Chen Q, Wang HJ, Zhang HQ. Condensation of a hydrocarbon in the presence of a non-condensable gas: heat and mass transfer. Appl Therm Eng 2015;91:938–45. https://doi.org/10.1016/j.applthermaleng.2015.08.092.
[17] Kandlikar SG, Shōji M, Dhir VK. Handbook of phase change: Boiling and condensationvol. 1. Taylor & Francis; 1999.
[18] Incropera F, DeWitt D, Bergman T, Lavine A. Fundamentals of heat and mass transfervol. 6. New York: Wiley; 1996.
[19] Rohsenow WM. A method of correlating heat-transfer data for surface boiling of liquids. J Fluids Eng 1952;74:969–75. https://doi.org/10.1115/1.4015984.
[20] Collier J, John Thome. Convective boiling and condensation. 3rd ed. NEw York: Oxford University Press; 1996.
[21] John Chato. Laminar condensation inside horizontal and inclined tubes (Doctoral dissertation, Massachusetts Institute of Technology). PhD Thesis. Massachusetts Institute of Technology; 1960.
[22] Holman JP. Heat transfer. 10th ed. New York: McGraw-Hill; 2010.
[23] Jin Z, Tian B, Wang L, Wang R. Comparison on thermal conductivity and permeability of granular and consolidated activated carbon for refrigeration. Chin J Chem Eng 2013;21:676–82. https://doi.org/10.1016/S1004-9541(13)60525-X.
[24] Wang X, Guo R, Xu D, Chung J, Kaviany M, Huang B. Anisotropic lattice thermal conductivity and suppressed acoustic phonons in MOF-74 from first principles. J Phys Chem C 2015;119:26000–8. https://doi.org/10.1021/acs.jpcc.5b08675.
[25] Yu H, Zhang H, Zhao J, Liu J, Xia X, Wu X. The thermal conductivity of micro/nano-porous polymers: Prediction models and applications. n.d.. 2024.
[26] Flynn Ann Marie, Akashige Toshihiro, Theodore Louis. Kern's process heat transfer. 2nd ed. New Jersey: Wiley; 2018.
[27] García-Mariaca A, Llera E. Dynamic CO2 capture in a natural gas engine used in road freight transport. SSRN Electron J 2022. https://doi.org/10.2139/ssrn.4272013.
[28] Hofmann E, Maucher D, Hornstein J, den Ouden R. Capital equipment purchasingvol. 2. Berlin, Heidelberg: Springer Berlin Heidelberg; 2012. https://doi.org/10.1007/978-3-642-25737-7.
[29] Wang N, Verzijlbergh RA, Heijnen PW, Herder PM. Incorporating indirect costs into energy system optimization models: application to the Dutch national program regional energy strategies. Energy 2023;276:127558. https://doi.org/10.1016/j.energy.2023.127558.
[30] Chang C, Liao Z, Costa ALH, Bagajewicz MJ. Globally optimal design of intensified shell and tube heat exchangers using complete set trimming. Comput Chem Eng 2022;158:107644. https://doi.org/10.1016/j.compchemeng.2021.107644.
[31] Robin Smith. Chemical process: Design and integration. West Sussex: John Wiley & Sons; 2005.
[32] Shamoushaki M, Niknam PH, Talluri L, Manfrida G, Fiaschi D. Development of cost correlations for the economic assessment of power plant equipment. Energies (Basel) 2021;14:2665. https://doi.org/10.3390/en14092665.
[33] Astolfi M. Techno-economic optimization of low temperature CSP systems based on ORC with screw expanders. Energy procediavol. 69. Elsevier Ltd; 2015. p. 1100–12. https://doi.org/10.1016/j.egypro.2015.03.220.
[34] Quoilin S, Declaye S, Tchanche BF, Lemort V. Thermo-economic optimization of waste heat recovery organic Rankine cycles. Appl Therm Eng 2011;31:2885–93. https://doi.org/10.1016/j.applthermaleng.2011.05.014.
[35] Cox B, Innis S, Steen J, Kunz N. The environmental and economic case for valuing water recovery and its relationship with tailings storage conservation. Miner Eng 2023;201:108157. https://doi.org/10.1016/j.mineng.2023.108157.
[36] De Saint Jean M, Baurens P, Bouallou C, Couturier K. Economic assessment of a power-to-substitute-natural-gas process including high-temperature steam electrolysis. Int J Hydrogen Energy 2015;40:6487–500. https://doi.org/10.1016/j.ijhydene.2015.03.066.
[37] Peters Max Stone, Timmerhaus Klaus D. Plant desing and economics for chemical engineers. McGraw-Hill Companies; 1990.
[38] Abu-Zahra MRM, Niederer JPM, Feron PHM, Versteeg GF. CO2 capture from power plants. Part II. A parametric study of the economical performance based on mono-ethanolamine. Int J Greenh Gas Control 2007;1:135–42. https://doi.org/10.1016/S1750-5836(07)00032-1.
[39] Bailera M, Espatolero S, Lisbona P, Romeo LM. Power to gas-electrochemical industry hybrid systems: a case study. Appl Energy 2017;202:435–46. https://doi.org/10.1016/j.apenergy.2017.05.177.
[40] Gasolineras GNC. Guía de Precios actualizada a diario. https://www.gasolinerasgnc.com/; 2024.
[41] Alshammari F, Karvountzis-Kontakiotis A, Pesyridis A, Usman M. Expander technologies for automotive engine Organic Rankine cycle applications. Energies (Basel) 2018;11:1905. https://doi.org/10.3390/en11071905.
[42] López JJ, Novella R, Gomez-Soriano J, Martinez-Hernandiz PJ, Rampanarivo F, Libert C, et al. Advantages of the unscavenged pre-chamber ignition system in turbocharged natural gas engines for automotive applications. Energy 2021;218:119466. https://doi.org/10.1016/j.energy.2020.119466.
[43] Cengel Yunus A. Heat and transfer: A practical approach. 2nd ed. McGraw-Hill Education; 2004.
[44] Tlili N, Grévillot G, Vallières C. Carbon dioxide capture and recovery by means of TSA and/or VSA. Int J Greenh Gas Control 2009;3:519–27. https://doi.org/10.1016/j.ijggc.2009.04.005.
[45] Mercedes-Benz. Citaro NGT technical information. 2017. p. 1–16.
[46] Iveco company. IVECO DAILY technical information. https://www.iveco.com/Denmark/Documents/Configurator/Brochure/Dailyvan_DK.pdf; 2015 (accessed February 8, 2023).

[47] Ally J, Pryor T. Life cycle costing of diesel, natural gas, hybrid and hydrogen fuel cell bus systems: an Australian case study. Energy Policy 2016;94:285–94. https://doi.org/10.1016/j.enpol.2016.03.039.
[48] Holland SP, Mansur ET, Muller NZ, Yates AJ. The environmental benefits of transportation electrification: urban buses. Energy Policy 2021:148. https://doi.org/10.1016/j.enpol.2020.111921.
[49] Spendelow J, Papageorgopoulos D, Satyapal S. Fuel cell technologies program record 12012: Fuel cell bus targets. 2012.
[50] Quarles N, Kockelman KM, Mohamed M. Costs and benefits of electrifying and automating bus transit fleets. Sustainability 2020;12:3977. https://doi.org/10.3390/su12103977.
[51] Fleet Owner. Pricing set for GM's CNG vans. https://www.fleetowner.com/emissions-efficiency/article/21662580/pricing-set-for-gms-cng-vans; 2010.
[52] Wątróbski J, Małecki K, Kijewska K, Iwan S, Karczmarczyk A, Thompson R. Multi-criteria analysis of electric vans for city logistics. Sustainability 2017;9:1453. https://doi.org/10.3390/su9081453.
[53] Jones J, Genovese A, Tob-Ogu A. Hydrogen vehicles in urban logistics: a total cost of ownership analysis and some policy implications. Renew Sustain Energy Rev 2020;119:109595. https://doi.org/10.1016/j.rser.2019.109595.
[54] Haywood L, Jakob M. The role of the emissions trading scheme 2 in the policy mix to decarbonize road transport in the European Union. Transp Policy (Oxf) 2023;139:99–108. https://doi.org/10.1016/j.tranpol.2023.06.003.
[55] Cerrera Iñaki. El transporte por carretera pagará por sus emisiones de carbono a partir de 2027. https://elmercantil.com/2022/12/22/el-transporte-por-carretera-pagara-por-sus-emisiones-de-carbono-a-partir-de-2027/; 2022 (accessed March 30, 2024).
[56] Zhou T, Roorda MJ, MacLean HL, Luk J. Life cycle GHG emissions and lifetime costs of medium-duty diesel and battery electric trucks in Toronto, Canada. Transp Res D Transp Environ 2017;55:91–8. https://doi.org/10.1016/j.trd.2017.06.019.
[57] Perpiñán J, Bailera M, Peña B, Romeo LM, Eveloy V. Technical and economic assessment of iron and steelmaking decarbonization via power to gas and amine scrubbing. Energy 2023;276:127616. https://doi.org/10.1016/j.energy.2023.127616.
[58] Barón C, Perpiñán J, Bailera M, Peña B. Techno-economic assessment of glassmaking decarbonization through integration of calcium looping carbon capture and power-to-gas technologies. Sustain Prod Consum 2023;41:121–33. https://doi.org/10.1016/j.spc.2023.07.029.